Journal of Biomechanics 205 (2026) 113420

Contents lists available at ScienceDirect

Journal of Biomechanics

journal homepage: www.elsevier.com/locate/jbiomech

Scaling contact force parameters across body size, limb count, and number of contact spheres

Pasha A. van Bijlert [a, b]

[a] Department of Earth Sciences, Faculty of Geosciences, Utrecht University, Vening Meinesz Building A, Princetonlaan 8A, 3584 CB, Utrecht, the Netherlands
[b] Naturalis Biodiversity Center, Darwinweg 2, 2333 CR, Leiden, the Netherlands

ARTICLE INFO

Keywords:
Contact mechanics
Scaling
Impacts
Musculoskeletal modelling
Dynamic similarity
Allometry

ABSTRACT

Dynamic simulations of contact interactions involve a trade-off between realism and numerical performance. Contact interactions in musculoskeletal simulations are often modelled using Hertz theory applied to contact spheres, with Hunt–Crossley based dissipation. Suitable contact parameters are highly dependent on the morphology, scale, materials, and movement in question. Inappropriate parameter choices can manifest in unpredictable ways, potentially resulting in misinterpretations or failed simulations.

Here, I demonstrate that the plane strain modulus and dissipation parameters are not scale invariant. I derive equations to scale the contact parameters in dimensionless form, which allows accounting for differences in body size, contact sphere radius, number of contacting elements (e.g., limb count), and number of spheres. As a demonstration of this approach, I scale the contact parameters of a 62 kg human to a 500 kg human, a mouse (0.02 kg), an emu (37.8 kg), a horse (545 kg), and a giraffe (1190 kg). Geometrically and dynamically similar contact behaviour is achieved in all cases.

The equations presented here can be used to derive contact parameters in a variety of ways, including scaling parameters between different models (useful when simulating the effects of allometric scaling), and estimating suitable contact parameters directly from force-displacement curves. The limitations of Hertz–Hunt–Crossley contact models are discussed, and I provide some strategies to navigate the trade-offs inherent to their use in biomechanical simulations. Lastly, I derive dimensionless expressions and scaling guidelines for the smoothed contact force implementation "SmoothSphereHalfSpaceForce" in the popular simulator OpenSim.

1. Introduction

Dynamic simulations of musculoskeletal models have a wide variety of fundamental and clinical applications in biomechanics (van Soest et al., 1993; van den Bogert et al., 1989; Sellers et al., 2013; Bianco et al., 2023). It is often required to model contact interactions, for example to acquire ground reaction forces during locomotion (van den Bogert et al., 1989; Sellers et al., 2013; Bianco et al., 2023; Clemente et al., 2024; Bates et al., 2025), reaction forces when manipulating objects (Hao and Nichols, 2021), or forces on the teeth during biting (Watson et al., 2014; Bates and Falkingham, 2012). A popular approach to achieve this is using contact spheres (Sherman et al., 2011; Seth et al., 2018; Rodrigues Da Silva et al., 2022). When these spheres intersect with other spheres or a halfspace (i.e., a plane), the elastic portion of the forces is computed following Hertz theory of elastic contact (Hertz, 1896; Johnson, 1985; Sherman et al., 2011).[1] Dissipation is incorporated as a function of both the elastic force and the intersection speed, using the Hunt–Crossley model (Hunt and Crossley, 1975).

Theory and physical experiments have shown that substrate compliance can have profound effects on locomotor performance and energetics (McMahon and Greene, 1979; Kerdok et al., 2002). This has important consequences for biomechanical simulations, where contact models are often used to represent combined deformations in the contacting tissue and substrate. The contact parameters can affect simulated kinematics (D'Hondt et al., 2024a) and energetics (Grant et al., 2022; Afschrift et al., 2025), given that contact forces tend to be modelled as

Email address: a.m.vanbijlert@uu.nl, pasha.vanbijlert@naturalis.nl.

[1] Hertz derived what is now known as Hertz theory of elastic contact at the age of 23 during his Christmas break in 1880, essentially starting the field of contact mechanics (Johnson, 1985). He is better-known for conducting experiments demonstrating the existence of electromagnetic waves (Hertz, 1893), which is honoured by the eponymous SI-unit Hz.

https://doi.org/10.1016/j.jbiomech.2026.113420
Accepted 15 June 2026
Available online 19 June 2026

one of the major sources of energy dissipation in the system (Afschrift et al., 2025).

Contact parameters can introduce a trade-off between realism and numerical performance (van den Bogert et al., 1989). Simulations using the published bird model from van Bijlert et al. (2024b) illustrate these effects (Fig. 1, see methods and supplementary text for details). Plane strain modulus E^* affects the contact stiffness, and α affects energy dissipation (these parameters are explained in more detail later in this manuscript). Fig. 1(A) shows that E^* and α have systematic effects on the energetic cost of transport. Most notably, high E^* increases mechanical stiffness and decreases costs, whereas at low E^*, the dissipation parameter strongly increases costs. These parameters have the opposite effect on iteration times (Fig. 1B). Mechanical stiffness in the contacts results in numerically stiff differential equations, a numerically undesirable phenomenon that can result in longer computation times regardless of the solver method used (van den Bogert et al., 1989; Hao and Nichols, 2021; De Groote et al., 2016; van den Bogert et al., 2011). A much more insidious problem arises when attempting to simulate new gaits for a model where no previous gait solutions exist: the optimiser will be much more likely to fail or find local optima when using stiff contact parameters (Fig. 1C). Conversely, very compliant contacts tend to be easier to simulate (Fig. 1C), but break the assumptions underlying the Hertz model (Johnson, 1985) and may also overestimate costs (Fig. 1A). Thus, inappropriate contact parameters can have negative effects on simulations, which could be misinterpreted as biologically meaningful results, or simply cause failed simulations, which may be misattributed to other model tuning issues.

Unfortunately, judicious parameter selection is not straightforward when using contact spheres. Often, the composite plane strain modulus E^* (in N / m^2) is incorrectly treated as equivalent to "stiffness" (in N / m). However, E^* depends solely on material properties (see Appendix A), and is size invariant unless a specific scaling approach is employed. In contrast, stiffness depends on both material and structural properties, and varies with sphere size even if E^* is constant (see Appendix B). Similarly, the Hunt–Crossley dissipation parameter α affects the coefficient of restitution in a scale dependent way. These complexities make it difficult to anticipate the physical and numerical effects of the contact parameters, especially when simulating a model for the first time.

Here, I derive scaling equations for contact parameters based on Hertz theory of elastic contact, combined with Hunt–Crossley dissipation. These equations provide a clearer theoretical basis for contact parameter selection, and are intended to support more informed and consistent choices when used in simulations. The scaling equations result in geometrically and dynamically similar contact sphere interactions at different body sizes, numbers of spheres per foot, and contact radii, allowing for size-invariant contact behaviour. I will demonstrate the effects of this scaling using simulated drop tests of a variety of animal models of varying body sizes and shapes (Fig. 2). Simulations were performed using the popular simulator OpenSim (Seth et al., 2018; Dembia et al., 2020), which implements Hertz-style contacts (with Hunt–Crossley-style dissipation (Hunt and Crossley, 1975)) as both "HuntCrossleyForce" and "SmoothSphereHalfSpaceForce". Additional derivations for size-invariant behaviour of "SmoothSphereHalfSpaceForce" are presented in Appendix C. While this manuscript is primarily concerned with contact interactions in musculoskeletal systems, the underlying scaling principles are general and applicable to any system modelling Hertzian elastic contact with Hunt–Crossley inspired dissipation.

2. Theory and derivations

Sherman et al. (2011) described an implementation of elastic contact between two non-conforming bodies, based on Hertz theory as outlined by Johnson (1985). The elastic (velocity-independent) portion of the contact force (F_e, in N) is calculated as:

$$F_e = \frac{4}{3}\eta \cdot R^{1/2} \cdot E^* \cdot x^{3/2} \tag{1}$$

Here, η is 1 when using contact spheres (Sherman et al., 2011), and in general depends on the shape of the colliding objects (Johnson, 1985). Sherman et al. (2011) used the symbol σ instead of η, but in this manuscript σ denotes stress. R is a composite radius (in m); when modelling contact between a sphere and a halfspace (a plane), radius R is equal to the radius of the sphere (Fig. 3). x is the combined indentation of the two objects (in m), equal to the total intersection distance if the objects could interpenetrate. x thus measures how much total deformation occurs during the contact. E^* is the composite plane strain modulus (in N / m^2) of two colliding objects that have Young's modulus E_1 and E_2, respectively (in N / m^2). See Appendix A for details

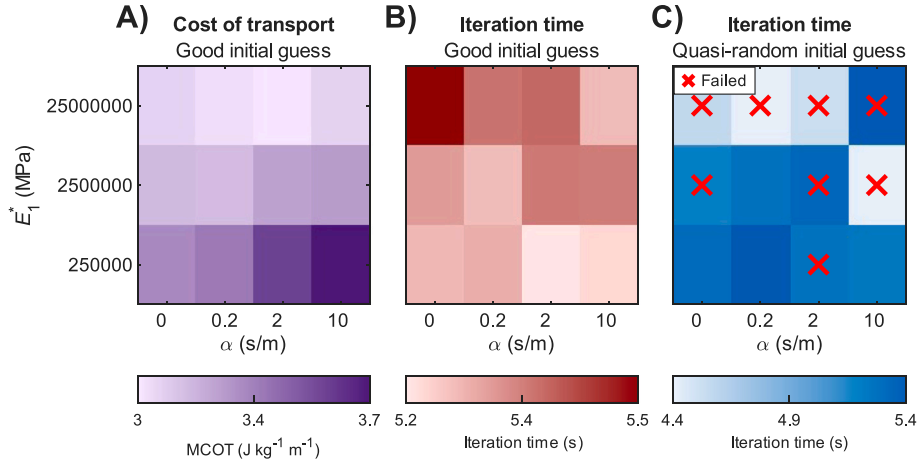

Fig. 1. Contact parameters have both biologically and numerically relevant effects. These figures show gait simulations of the bird model from van Bijlert et al. (2024b), subjected to a parameter sweep of E_1^* (plane strain modulus, higher E_1^* makes the contacts stiffer), and α (energy dissipation). **A)** When starting optimisations from a good initial guess, high E_1^* reduces metabolic cost of transport (MCOT), whereas high α tends to raise MCOT. **B)** The same simulations from panel A show the opposite effect on iteration times: high E_1^* tends to increase iteration times, and high α tends to reduce them. **C)** When using a quasi-random initial guess, which mimics the situation of simulating a new model for the first time, stiff contacts can lead to failed optimisations (here defined as failure to converge within 3000 iterations). See the supplementary text for more details and extra outputs of these simulations.

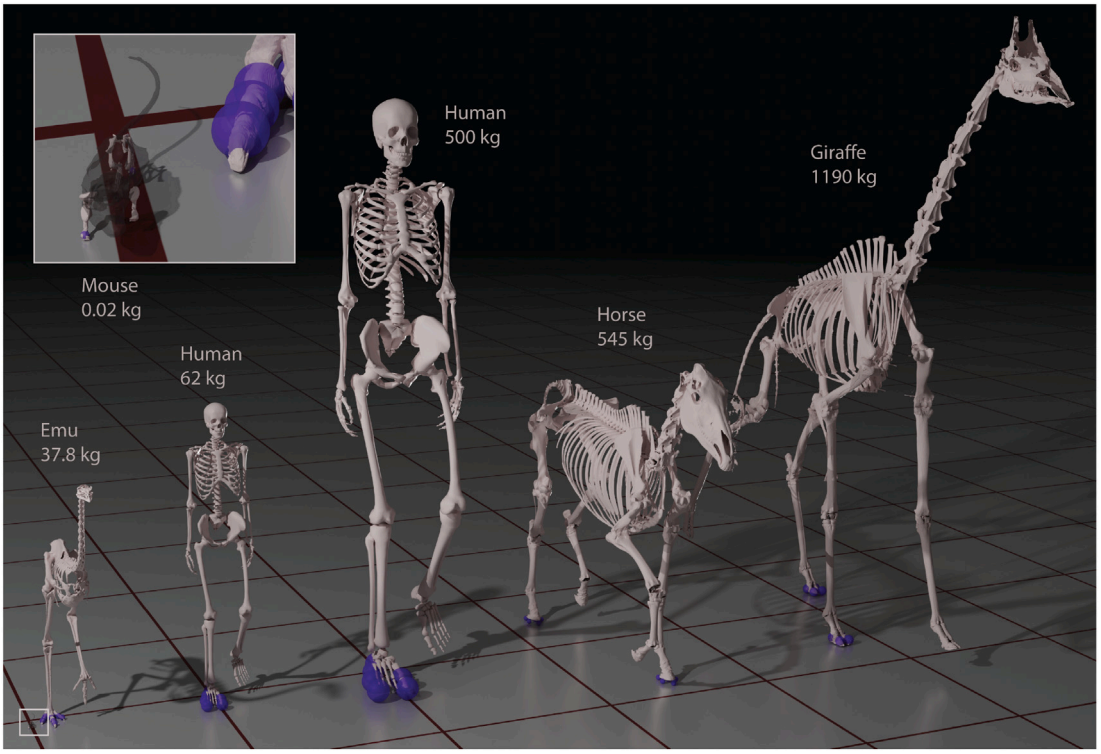

Fig. 2. Models with different body sizes, limb counts, and numbers of contact spheres (in purple) were subjected to a simulated drop test to evaluate the effect of scaling the contact parameters. Two variants of the emu model were simulated (with 10 and 2 contact spheres), but only one is pictured. The inset depicts the mouse model, with one of the emu toes for scale. The quadrupedal models were posed so that two limbs contacted the ground (with varying numbers of contact spheres in total, see Table 1). The ground plane has a 1×1 m grid.

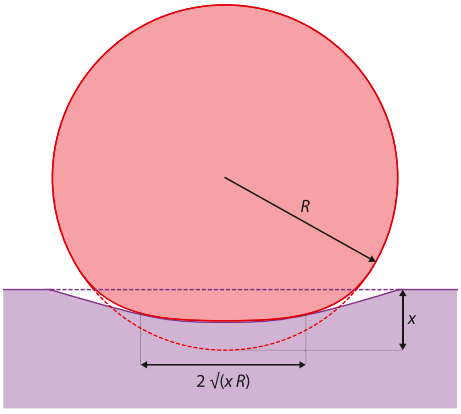

Fig. 3. Contact interaction between a sphere with radius R and a halfspace. The indentation x is the total intersection distance between the two objects if they would not deform. The contact patch between a sphere and a halfspace is circular and has diameter $2\sqrt{xR}$, for small x.

on how to convert Young's modulus E into plane strain modulus E^*, and for the combining rules for constructing composite moduli. How the total deformation x maps into the individual deformations of the two objects depends on their relative material properties and geometries (Johnson, 1985; Sherman et al., 2011), and will not be elaborated on here. OpenSim users should note that they do not directly input E^* (the composite plane strain modulus), but E_1^* (the plane strain modulus of one of the colliding objects), which has consequences for the material properties being simulated (see Appendix A for details).

To achieve size-invariant behaviour, it is convenient to scale x by R to acquire a dimensionless expression for relative deformation:

$$\hat{x} = \frac{x}{R} \quad \Rightarrow \quad x = \hat{x} \cdot R, \tag{2}$$

which allows us to re-express the original equation:

$$F_e = \frac{4}{3}\eta \cdot R^{1/2} \cdot E^* \cdot (\hat{x} \cdot R)^{3/2}$$

$$F_e = \frac{4}{3}\eta \cdot R^2 \cdot E^* \cdot \hat{x}^{3/2} \tag{3}$$

We will assume the force F_e represents the ground reaction force in static equilibrium, and thus scales with body mass M. We also assume that this force is equally distributed across several spheres, which all have equal radius and lie on the same plane. This gives:

$$F_e \propto \frac{M}{n_{\text{spheres}}}. \tag{4}$$

n_{spheres} is the investigator's arbitrary selection of number of spheres per foot. From Eq. (3), the following proportionality is clear:

$$F_e \propto R^2\, E^*\, \hat{x}^{3/2} \tag{5}$$

Next, we can combine this with Eq. (4) to derive the following proportionality:

$$\frac{M}{n_{\text{spheres}}} \propto E^* \cdot \hat{x}^{3/2} \cdot R^2 \tag{6}$$

To enforce the same relative indentation irrespective of size (i.e., geometric similarity (Alexander, 2006)), we treat $\hat{x}$ as a constant. We

are left with:

$$\frac{M}{n_{\text{spheres}}} \propto E^* \cdot R^2 \tag{7}$$

Now we can rewrite for E^*, assuming constant $\hat{x}$:

$$E^* \propto \frac{M}{n_{\text{spheres}} \cdot R^2} \tag{8}$$

If we assume R scales with the linear dimensions of the model ($R \propto M^{1/3}$), then E^* scales with $M^{1/3}$ when relative indentation $\hat{x}$ is kept constant. This may seem surprising, given that the material properties of biological tissues generally do not vary with size. However, in this context the plane strain modulus E^* represents the combined effects of multiple tissues (and possibly even the substrate), and their relative compositions may indeed vary with size. For example, the Young's modulus of a small sample of carnivoran footpads has been shown to scale with $M^{0.59}$ and $M^{0.39}$ (fore and hind, respectively) (Chi and Louise Roth, 2010). This supports the notion that deriving E^* based on properties of individual tissues may yield inconsistent results in musculoskeletal simulations. In situations where the contact forces do not represent body weight but some other external force (e.g., biting), M in Eq. (8) can be replaced with F_{expected} (see section 2.2).

2.1. Scaling E^* between models

The composite plane strain modulus E^* (in N /m^2) represents the combined effect of the material properties of the two colliding objects. Using Eq. (8), we can scale E^* from model a to differently sized model b by defining the following:

$$\frac{E_b^*}{E_a^*} = \left(\frac{M_b}{M_a}\right) \cdot \left(\frac{n_{\text{spheres},a}}{n_{\text{spheres},b}}\right) \cdot \left(\frac{R_a^2}{R_b^2}\right) \tag{9}$$

This applies when the sphere forces are proportional to body mass (e.g., contact forces arising from body weight and/or inertial effects, such as ground reaction forces). The final expression for scaling composite plane strain modulus is:

$$E_b^* = \left(\frac{M_b}{M_a}\right) \cdot \left(\frac{n_{\text{spheres},a}}{n_{\text{spheres},b}}\right) \cdot \left(\frac{R_a^2}{R_b^2}\right) \cdot E_a^* \tag{10}$$

In general, the individual deformations in the sphere and plane will depend on their respective material properties (Appendix A, Sherman et al. (2011); Johnson (1985)). Because of the identical material assumption in OpenSim (Eq. A.4), Eq. (10) can also be applied to scale the individual plane strain moduli of the individual objects (i.e., E_1^*), which is what OpenSim users input.

2.2. Estimating a suitable E^* for an expected force magnitude

Eqs. (3) and (4) can also be combined to find a suitable E^* without scaling from a reference model, if we have an a priori expectation of the combined force magnitude F_{expected} in the spheres:

$$E^* = \frac{3\,F_{\text{expected}}}{4 \cdot \eta \cdot R^2 \cdot \hat{x}^{3/2} \cdot n_{\text{spheres}}}. \tag{11}$$

η is 1 for spherical contact, and is only included for completeness. Clearly, all the parameters on the right side are known except for the relative indentation $\hat{x}$. This allows us to set $\hat{x}$ to some desired level between 0 and 1, and calculate the magnitude of E^* that would achieve this. In other words, this equation calculates the required plane strain modulus to achieve a predetermined relative indentation in the contact spheres.

F_{expected} is situation and model dependent. For instance, it could represent biting force, or when performing gait simulations, F_{expected} could be set to a multiple of bodyweight to represent the ground reaction force. OpenSim users are reminded that since they define E_1^* in their models, the result of Eq. (11) should be multiplied by 2^n before being used as an input for their models (see Eq. (A.4)).

2.3. Constant coefficient of restitution

Dynamically similar contact behaviour implies that the coefficient of restitution c_r is constant between models. However, the coefficient of restitution is generally not specified directly when simulating contact spheres. Instead, damping is often included in the contact models using a Hunt–Crossley formulation (Hunt and Crossley, 1975; Sherman et al., 2011; Serrancoli et al., 2019; Rodrigues Da Silva et al., 2022). In the original Hunt–Crossley model, the damping force F_{d} is calculated as:

$$F_{\text{d}} = 3/2 \cdot F_{\text{e}} \cdot \alpha \cdot \dot{x}. \tag{12}$$

F_{e} and F_{d} are summed to acquire the total contact (normal) force. α, in units s / m, is a parameter that is related to the coefficient of restitution c_r as follows:

$$c_r = 1 - \alpha \cdot \dot{x}^{(-)}, \tag{13}$$

with $\dot{x}^{(-)}$ being the velocity before impact (Hunt and Crossley, 1975; Gonthier et al., 2004; Rodrigues Da Silva et al., 2022). This is an approximation that is valid for relatively low speeds and high magnitudes of c_r (Hunt and Crossley, 1975; Gonthier et al., 2004; Rodrigues Da Silva et al., 2022). Eq. (13) shows that the (approximate) coefficient of restitution c_r is solely dependent on the impacting speed. However, if two differently sized animals are moving according to dynamic similarity (Alexander and Jayes, 1983; Daley and Birn-Jeffery, 2018), their speeds would be proportional to the square root of a characteristic length. In other words: $\dot{x}^{(-)} \propto M^{1/6}$, or $\dot{x}^{(-)} \propto R^{1/2}$. This implies that if the parameter α (implemented in OpenSim as "dissipation") is kept constant for differently scaled models, the coefficients of restitution would not be identical at dynamically similar speeds. To keep the coefficient of restitution constant, $\alpha\dot{x}^{(-)}$ should be scale invariant. This is achieved by:

$$\alpha \propto M^{-1/6} \propto R^{-1/2}. \tag{14}$$

3. Methods

Models of a variety of different animals, encompassing a body mass of 0.02 - 1190 kg, were taken from the literature, or constructed for this study (Table 1, Fig. 2). The models were chosen to encompass a wide spread in morphologies, and size, and were deliberately modelled with different n_{spheres}. The human model from Falisse et al. (2022), scaled for Clemente et al. (2024) was provided courtesy of Christofer Clemente. The mouse model from Charles et al. (2016, 2024) was used, with a repositioned forelimb. The emu model was described in van Bijlert et al. (2024b), and the horse model in van Bijlert et al. (2024a). The giraffe model was created in Blender (blender.org) using MuSkeMo (van Bijlert, 2024), and was based on a 3D surface scan of a skeleton, as well as a body mass measured using scales in a different specimen (euthanised for reasons unrelated to this study). All models had contact spheres on the same plane, and modifications were made using MuSkeMo if required.

The parameters for the 62 kg human model have been used successfully in gait simulations (Falisse et al., 2022). For this study, plane strain moduli of all the other models were scaled according to Eq. (10) to match the 62 kg human model. Unidimensional vertical drop tests were simulated under the influence of gravity on Earth (g), because this experimental design isolates the dynamic behaviour of the contacts without possible interaction effects from (muscle) actuation. All models had only a single degree of freedom (vertical position), defined to be zero when the ground contact intersection commences. The final positions after 2 s were used to determine the final $\hat{x}$, which was enough time for oscillations to have been damped out. All models were dropped from a height of $0.25R$. To evaluate the effect of scaling α (the Hunt–Crossley dissipation parameter), the vertical contact forces were also extracted from the simulations. These were plotted against regular time (T), and against non-dimensional time, defined as $\frac{T}{\sqrt{R/g}}$ (see Appendix B, and (Daley and Birn-Jeffery, 2018)).

Table 1
Model parameters and results from the simulated drop tests. The model parameters are described in the text. Two sets of simulations were performed, one with constant α across all models, and one with scaled α. Because the final equilibrium indentation ($\hat{x}$) and equilibrium stiffness (k) were the same in both modalities due to the applied scaling, they are only reported once. † These models were posed so that two limbs were in contact with the ground, and the $n_{spheres}$ of both feet are reported together.

Taxon	Mass (kg)	$n_{spheres}$	R (m)	E^* (MPa)	E_1^* (MPa)	base α (s/m)	$\alpha \propto R^{-0.5}$ (s/m)	final $\hat{x}$	k (kN/m)
Human *Homo sapiens*	62	6	0.032	0.354	1.00	2.00	2.00	0.353	13.4
Human *Homo sapiens*	500	6	0.0637	0.720	2.04	2.00	1.42	0.353	54.5
Mouse† *Mus musculus*	0.0209	2	0.002	0.0916	0.259	2.00	8.00	0.353	0.218
Emu *Dromaius novaehollandiae*	37.80	10	0.015	0.589	1.66	2.00	2.92	0.353	10.5
Emu *Dromaius novaehollandiae*	37.80	2	0.030	0.736	2.08	2.00	2.07	0.353	26.2
Horse† *Equus ferus caballus*	545	10	0.015	8.49	24.0	2.00	2.92	0.353	151
Giraffe† *Giraffa camelopardalis*	1190	8	0.030	5.79	16.4	2.00	2.07	0.353	207

Simulations with α scaled according to Eq. (14) were compared to simulations where $\alpha = 1$ across all models. Simulations were performed in OpenSim 4.5 (Seth et al., 2018), using the MATLAB (Mathworks, Natick) API. The contact forces were modelled with the "HuntCrossleyForce" contact model, which incorporates Hertz theory and Hunt–Crossley dissipative forces (Sherman et al., 2011).

Detailed methods and supplementary results for the simulations in Fig. 1 are provided in a supplementary text. In short, the bird model and simulation code from van Bijlert et al. (2024b) were subjected to a parameter sweep of E_1^* and α. Optimisations were performed using direct collocation, as implemented in OpenSim Moco v4.5 (Dembia et al., 2020; Seth et al., 2018). The parameter sweep was performed at a target velocity of 1.25 m/s (walking speed), using an initial guess of a previously converged walking simulation from van Bijlert et al. (2024b), and using a quasi-random initial guess ("good" and "quasi-random" initial guesses, respectively). The good initial guesses always converged to a walking gait, whereas the quasi-random initial guesses sometimes converged to walking gaits, local optima or did not converge at all (Fig. 1, and see supplementary text).

4. Results and discussion

4.1. Equilibrium behaviour

Using Eq. (10) to scale the respective plane strain moduli, all the models had the same relative indentation $\hat{x}$ at static equilibrium (Table 1, Supplementary Figs. S1–S7). Thus, the scaling approach achieves the desired invariance to scale, morphologies, and number of legs.

All models had a relative indentation of $\hat{x} = 0.353$, a result of scaling all models to match the 62 kg human contact parameters from Falisse et al. (2022). Note that this amount of indentation is very high—Hertz theory assumes very small deformations (Johnson, 1985; Lin et al., 2009). I am unaware of studies testing the accuracy of Hertz-theory at sphere sizes commonly used in musculoskeletal simulations, but microindentation studies suggest the Hertz relationship is accurate until a maximum contact patch radius of $0.4R$ (Lin et al., 2009). This corresponds to a maximal $\hat{x}$ of $\tilde{0}.16$ (see Fig. 3). Table 1 also shows the contact stiffnesses k for the individual spheres in each model (derived in Appendix B), which are all relatively compliant. For example, the 62 kg human model had $k = 13.5$ kN / m per sphere, with two spheres approximately representing the heel pad, resulting in a stiffness of 27 kN /m, whereas mechanical testing of the human heel pad results in stiffnesses that are between 30 and 50 times higher (Aerts et al., 1995). Similarly, dimensionless stiffness $\hat{k}$ for all the models was 4.24 (see Appendix B), whereas Alexander et al. (1986) measured $\hat{k}$ 3 to 13 times higher in mammalian foot pads. Although the contact model also represents ground compliance, which is not represented in the mechanical tests (Alexander et al., 1986), very low ground stiffness is unlikely in many experimental situations (e.g., locomotion on a force plate). Despite using a low contact stiffness, Falisse et al. (2022) achieved a very good match to empirical ground reaction forces and kinematics using the parameters from Table 1 in their 62 kg human model. However, D'Hondt et al. (2024a) were able to improve simulated kinematics by raising E^* tenfold, and Afschrift et al. (2025) recently pointed out that the baseline contact parameters used in Falisse et al. (2022) result in supraphysiological amounts of energy dissipation in the contact model (see Section 4.2). However, Fig. 1(C) shows that very high E^* can make gait optimisations more unpredictable when using quasi-random initial guesses.

It is possible to use Eq. (11) to prescribe the indentation to occur at a multiple of bodyweight (e.g., $\hat{x} = 0.16$ at twice bodyweight), which can keep indentations low. Furthermore, Eqs. (11) and (B.2) (from Appendix B) can be solved simultaneously to calculate pairs of suitable E^* and R for prescribed pairs of stiffness k and relative indentation $\hat{x}$. The effect would be to simultaneously prescribe stiffness and ensure indentations are within the Hertz regime. This could potentially lead to numerically undesirable stiff contact behaviour (Fig. 1)(van den Bogert et al., 1989; Hao and Nichols, 2021), depending on the model and task characteristics, which may pose a pragmatic choice between parameters that abide by the small indentations assumption of Hertz contact theory or parameters that are suitable for simulations. Increasing the dissipation parameter can somewhat offset the increased simulation time of stiff contacts (Fig. 1B), but high dissipation using the Hunt–Crossley model is also problematic (see Section 4.2). High indentations can be partially avoided by enlarging the contact sphere radius, with the downside that the spheres may then become substantially larger than the impacting tissues they are meant to represent (e.g., the heel pad). Alternatively, maximizing the number of contact spheres ($n_{spheres}$) for a given plane strain modulus would also serve to reduce contact indentations (Eq. 11), and adopting a rigid-foot model could eliminate indentations fully (Millard and Mombaur, 2019).

Hertz theory also assumes linear elastic materials (Johnson, 1985), whereas soft biological tissues tend to exhibit non-linear elastic ("hyperelastic") behaviour (Aerts et al., 1995; Lin et al., 2009). This suggests that the Hertz contact model is not capable of simultaneously matching measurements of tissue deformations and contact forces using measured tissue properties, especially since biological tissues generally undergo higher deformations than are permissible under the assumptions of Hertz theory. For this scenario, sphere-based contact solutions that permit large deformations and hyperelastic materials (Lin et al., 2009) could be adapted to musculoskeletal simulations. Alternative contact models could also be explored, including models that allow arbitrary contact geometry using three-dimensional meshes (e.g., elastic foundation models (Johnson, 1985; Sherman et al., 2011) or models such as those described by Gong et al. (2025)), preferably with customisable load-deflection curves. However, smooth and twice-differentiable formulations of more elaborate contact models have not been implemented, to my knowledge, which would prevent their use in gait prediction with direct collocation using gradient-based optimisers (Dembia et al., 2020; Serrancoli et al., 2019; D'Hondt et al., 2024b).

The arguments presented above do not imply that the Hertz model must always be avoided in biological simulations. Indeed, the Hertz model's popularity partly stems from its ability to produce realistic

contact forces in a wide variety of contexts and parameter combinations (Hao and Nichols, 2021; Grant et al., 2022; Falisse et al., 2022; van Bijlert et al., 2024b; Clemente et al., 2024; van Bijlert et al., 2024a; D'Hondt et al., 2024a). However, at high relative contact indentations, the model should perhaps be viewed as an abstract non-linear spring, rather than an accurate simulation of colliding spheres with prescribed material properties. The deformations can then be thought to represent the combined effects of the material interactions, substrate deformations, and conformational changes in the skeletal structures that in reality have more mobility than degrees of freedom in the model (e.g., models with rigid toe segments). Nevertheless, given the profound influence of substrate compliance on movement (McMahon and Greene, 1979; Kerdok et al., 2002; Grant et al., 2022), future work could be aimed at systematically evaluating how contact parameter scaling influences gaits acquired using dynamic optimisation.

4.2. Dynamic behaviour

Without scaling the dissipation parameter α, the dynamic behaviour of the models varied strongly with size (Fig. 4, Supplementary Figs. S1-S7). This can be most clearly observed in the mouse simulations: at $\alpha = 2$ s / m, the model oscillated around the equilibrium indentation, and was thus underdamped with respect to the other models (Fig. 4A). After scaling α according to Eq. (14), all models behaved in a dynamically similar manner (Fig. 4B), Supplementary Figs. S1-S7). These results demonstrate that without adjusting the dissipation parameter, models at different scales would experience proportionally different levels of energy loss during contact interactions. In the simple drop tests simulated here, the effective mass during the contact was simply the total body mass. In reality, the mass of the foot is only a small fraction of total body mass, and underdamped contacts could result in the feet bouncing off the ground after contact, which is not observed in real animals (Alexander et al., 1986). In a gait simulation, underdamped contacts could potentially lead to bouncing or oscillations of the feet, or compensatory actuation leading to increased positive or negative muscle work. This is problematic, because it is often differences in energy consumption or actuator use that are of interest in a simulation study (Miller et al., 2024; Afschrift et al., 2025; van Bijlert et al., 2024b; Grant et al., 2022; McConnochie et al., 2026). Thus, the dissipation parameter α should be scaled, especially when simulating models of particularly small animals.

The base value of dissipation used here ($\alpha = 2$ s / m) was chosen to match the human simulations by Falisse et al. (2022). This large amount of dissipation violates the assumptions of the Hunt–Crossley model—the Hunt–Crossley model is only accurate for high coefficients of restitution (i.e., $c_r \gtrsim 0.8$) (Hunt and Crossley, 1975; Gonthier et al., 2004; Skrinjar et al., 2018; Rodrigues Da Silva et al., 2022). By Eq. (13), a dissipation of 2 s/m is only modelled accurately at the scale of the mouse model (where $c_r = 0.8$). The 62 kg human model had a pre-impact velocity of approximately 0.4 m / s, suggesting a coefficient of restitution c_r of 0.2 (Eq. 13). $\dot{x}$ of 0.4 m/s implies a maximum permissible α of ~ 0.5 s/m. This pre-impact velocity is on the low-end for human walking (Baines et al., 2018), implying an even lower c_r in human gait simulations that used $\alpha = 2$ s / m (Falisse et al., 2022; D'Hondt et al., 2024a; Afschrift et al., 2025). As a result, contact dissipation may be inaccurately simulated when using high α at the scale of a human, which can have unpredictable effects on (muscle) actuation. This may have contributed to the finding by Afschrift et al. (2025) that high α resulted in overestimations of muscle work, and that raising E^* (while keeping α high and thus c_r low) did not fully resolve the issue.

The Hunt–Crossley model's failure to accurately model high dissipation (Gonthier et al., 2004; Skrinjar et al., 2018; Rodrigues Da Silva et al., 2022; Ding et al., 2024) is problematic for biological simulations, because dissipative contacts are necessary both for numerical stability, and to model realistic biological movements. For example, dissipation during heel-strike is thought to meaningfully contribute to the human metabolic cost of transport (Baines et al., 2018). Dynamic compression tests of the human heel pad suggest energy losses between 30.9 and 48.2 % (Aerts et al., 1995). This implies coefficients of restitution between 0.83 and 0.72, respectively, assuming measurements of energy return can be crudely approximated as $c_r{}^2$. Thus, the human heel pad can already be more dissipative than can be accurately modelled with the Hunt–Crossley model, without accounting for extra dissipation in the substrate. For highly dissipative contacts, alternatives or extensions to the Hunt–Crossley dissipative model may be more suitable (Gonthier et al., 2004; Skrinjar et al., 2018; Rodrigues Da Silva et al., 2022; Ding et al., 2024). However, this family of contact models currently cannot account for situations where the equilibrium indentation depth changes during the contact, such as during locomotion on deformable substrates (Prescott et al., 2025) or during mastication (Watson et al., 2014), which might require a two state contact model instead.

The proportionality in Eq. (14) allows for dynamically similar contact behaviour between models (Fig. 4), minimizing undesirable scale effects when comparing animal models of different sizes. Note that this does not necessarily achieve full dynamic similarity between models in gait simulations, which presupposes at least some degree of geometric similarity in the legs (Alexander, 2006). Even between similarly proportioned animals (e.g., two birds of different sizes), strict dynamic similarity in simulations would only be possible if the contact sphere radii were a constant proportion of leg length.

4.3. Recommendations for contact parameter selection

Research goals, morphology, material properties, and the simulation framework in use can all affect the ideal contact parameters, further

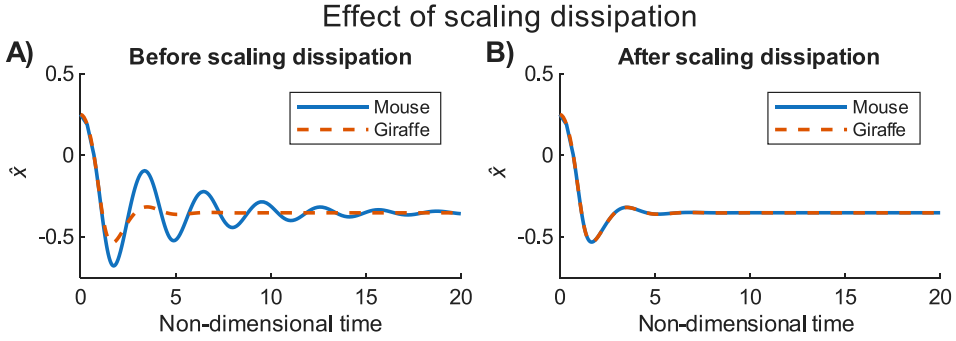

Fig. 4. Effect of scaling contact dissipation α. **A)** Before scaling, the contact behaviour was strongly size dependent, with smaller models being progressively more underdamped. This was most extreme in the mouse model, which showed a sustained oscillation around the equilibrium indentation. **B)** After scaling α, all models showed the same dynamic behaviour, here exemplified by comparing the mouse and giraffe simulations.

complicated by trade-offs between realism and numerical conditioning. This makes it challenging to provide unambiguous recommendations for contact parameter selection when using Hertz–Hunt–Crossley models. I will give a short summary of how the derivations and theory in this manuscript can be used for more informed contact parameter selection.

- Plane strain modulus E^* is not equivalent to stiffness k (see Appendix B). Changes to mass, proportions, or contacting spheres can be accounted for using Eq. (10) without changing the relative indentations of the contact spheres.
- It is possible to calculate the required E^* that matches a measured force-indentation combination using Eq. (11). Similarly, it is possible to calculate the required E^* that results in a local stiffness k using Eq. (B.2). These calculations are exact for single spheres, and for multiple spheres if they have the same radius and are distributed parallel to the contacting plane.
- Dissipation parameter α is not scale invariant (Fig. 4), if the impacting velocity is expected to follow dynamic similarity (e.g., locomotion under influence of gravity). The effects could become problematic at very small sizes, and can be resolved by scaling α according to Eq. (14).
- The assumptions of the Hertz model are violated when relative indentation $\hat{x}$ exceeds 0.16 (Johnson, 1985; Lin et al., 2009). This can be avoided by increasing sphere radius R, E^*, or number of contacting spheres, which all result in increased stiffness (Appendix B). Similarly, the assumptions of the Hunt–Crossley dissipation model are violated when the coefficient of restitution c_r is lower than 0.8 (Gonthier et al., 2004; Rodrigues Da Silva et al., 2022), corresponding to $\alpha \gtrsim 0.5$ s / m for slow human walking. Eq. (13) can be used to compute the maximum α for a given (expected) contact velocity $\dot{x}$. If the assumptions are violated, the model still behaves like a damped non-linear spring, but forces will not be representative of mechanical interactions with the specified material and dissipative properties. Thus, low E^* and low α are necessary for realistic mechanical interactions, but these result in the least favourable numerical conditions (Fig. 1, and van den Bogert et al. (1989)). In direct collocation using gradient-based optimisations (van den Bogert et al., 2011; De Groote et al., 2016), a possible strategy to navigate this is to initially search for good solutions using compliant contacts, and then raise E^* and reduce α in the final simulations. Computing non-dimensional stiffness $\hat{k}$ could aid this (Appendix B). For instance, the bottom row of simulations in Fig. 1(C) used $\hat{k} = 1.2$ at body weight. Alternatively, if realistic mechanical interactions using large deformations and/or dissipations are required, it could be advisable to use alternative formulations (Lin et al., 2009; Rodrigues Da Silva et al., 2022), or move away from sphere-based contact models altogether.
- If attempting to match stresses, for instance when using pressure plates (Michilsens et al., 2009), contact stress σ (in N / m^2) follows from the diameter of the contact patch area (see Fig. 3):

$$\sigma = \frac{F_e}{\pi \cdot R^2 \cdot \hat{x}} \tag{15}$$

  See also (Johnson, 1985; Lin et al., 2009).
- If attempting to derive a composite plane strain modulus E^* from Young's modulus and other material properties (e.g., such as in Grant et al. (2022)), the equations from Appendix A can be used. In many biomechanical scenarios, the resulting properties will likely violate the assumptions of the Hertz–Hunt–Crossley model (see above). E^* represents the mechanical effect of both objects, unless $E_1 \lll E_2$ or vice versa. OpenSim users are reminded that they specify E_1^*, not E^*, and this can lead to almost a factor three mismatch in expected versus modelled behaviour (Eq. A.4).
- The smoothed version of the Hertz–Hunt–Crossley model proposed by Serrancoli et al. (2019) for gradient-based optimisation has additional parameters that are not scale invariant, which is particularly problematic when using small contact spheres. This model is implemented as "SmoothSphereHalfSpaceForce" in OpenSim. Users of OpenSim Moco (Dembia et al., 2020) and Predsim (D'Hondt et al., 2024b) can use the dimensionless scaling approach outlined in Appendix C.

5. Conclusion

The equations and derivations presented here provide guidance for choosing scale-invariant contact parameters, following the principles of geometric and dynamic similarity. Both the plane strain modulus and dissipation parameters should be adjusted if large size-ranges are being investigated. OpenSim's tanh-smoothed contact model "SmoothSphereHalfSpaceForce" requires further scaling of the smoothing parameters to remain scale-invariant (see Appendix C). Due to the assumptions of small deformations and linear elasticity, the Hertz contact model should not be expected to provide perfect correspondences with simultaneously measured biological tissue deformations and contact forces. The original Hunt–Crossley dissipation model may not be adequate in simulations where high damping or other hysteresis effects are critical. As such, many biological contact interactions violate the assumptions underlying the Hertz–Hunt–Crossley model, whereas strict adherence to small deformations and low dissipations may introduce numerical stiffness. Thus, well-chosen contact parameters represent a trade-off between computational efficiency and realism. By aiming for dynamically similar contact behaviour, researchers can minimize inconsistencies between studies and across different model scales.

Funding

This research did not receive any specific grant from funding agencies in the public, commercial, or not-for-profit sectors.

Declaration of competing interest

The authors declare that they have no known competing financial interests or personal relationships that could have appeared to influence the work reported in this paper.

Acknowledgements

I thank Niklas Hohmann for discussions on the initial derivations, and Knoek van Soest for motivating me to explore the smoothed versions of the contact models. Karl Bates, Anne Schulp, two anonymous reviewers, and the editor provided helpful comments on this manuscript. I thank Nicholas Bianco and Antoine Falisse for clarifying the contact model implementations in OpenSim, and Friedl De Groote and Lars D'Hondt for further discussions on contact models in simulations. Christofer Clemente kindly shared the human models used in this manuscript, and James Charles shared additional 3D models which enabled repositioning of the mouse model. Claudia Wolschrijn of the Department of Clinical Sciences, Section Anatomy and Physiology (Utrecht University) provided permission to 3D scan the giraffe skeleton, and Jooske IJzer and Louis van den Boom, along with the staff at The Veterinary Pathology Diagnostic Centre (Utrecht University) provided the body mass measurement of a deceased giraffe. I am grateful to the Comparative Neuromuscular Biomechanics Technical Group for organising and inviting me to the Muscle-Tendon Mechanics Across Species ISB 2025 Satellite Meeting.

Appendix A. Plane strain modulus

For an object with Young's modulus E_1 and Poisson's ratio ν_1, its plane strain modulus E_1^* is computed as (Johnson, 1985):

$$E_1^* = E_1/(1 - \nu_1^2) \tag{A.1}$$

The composite plane strain modulus E^* can be constructed from the plane strain moduli of the two colliding objects. E^* is constructed using

either (Johnson, 1985):

$$E^* = \frac{E_1^* \cdot E_2^*}{E_1^* + E_2^*} \tag{A.2}$$

Alternatively, using the combining rule derived by Sherman et al. (2011), which is implemented in Simbody and OpenSim:

$$E^* = \left(\frac{E_1^{*2/3} \cdot E_2^{*2/3}}{E_1^{*2/3} + E_2^{*2/3}} \right)^{3/2} \tag{A.3}$$

By default, OpenSim assumes that both the colliding objects have the same plane strain modulus ($E_1^* = E_2^*$), in which case both objects deform equally and the force is applied halfway between both objects. Note that this implies that:

$$E_1^* = E_2^* = 2^n \cdot E^*, \tag{A.4}$$

with $n = 1$ when using Eq. (A.2) and $n = 3/2$ when using Eq. (A.3). This has consequences if the intended goal is to model the interactions using measured or estimated material properties, instead of the functional approach proposed in the main manuscript. For example, if the intention is to model the interaction between an animal's foot pad (i.e., a soft object with **m**easured Young's modulus $E_{1,\mathrm{m}}$), and a force plate or concrete (an object assumed to have effectively infinite stiffness), then in the limit for E_2^* to infinity in Eqs. (A.2) and (A.3):

$$E^* \to E_{1,\mathrm{m}}^* \quad \text{as } E_2^* \to \infty \tag{A.5}$$

Because in OpenSim, the input is E_1^* and not E^*, combining Eqs. (A.1), (A.4), and (A.5), OpenSim users should input $2^n \cdot \frac{E_{1,\mathrm{m}}}{1-\nu_1^2}$ as the plane strain modulus when starting from a measured Young's modulus, under the assumption that the other surface has an effectively infinite Young's modulus. Note that the force would still be applied halfway between the two colliding objects.

Appendix B. Contact force stiffness and natural frequency

Eq. (1) can be viewed as a non-linear spring. Stiffness k (in N/m) then follows as $\frac{\partial F}{\partial x}$:

$$k = 2 \cdot \eta \cdot R^{1/2} \cdot E^* \cdot x^{1/2} \tag{B.1}$$

Combining this with Eq. (2), we acquire:

$$k = 2 \cdot \eta \cdot R \cdot E^* \cdot \hat{x}^{1/2} \tag{B.2}$$

This shows that effective stiffness is linear in both R and E^*, at any given relative indentation. It is possible to solve Eqs. (11) and (B.2) as simultaneous equations, and use this to estimate suitable values for both E^* and R. This can be achieved by prescribing a desired stiffness k (in N/m) and a (maximum) relative indentation $\hat{x}$, and then solving for the unknown E^* and R.

Assuming R and E^* both scale with $M^{1/3}$ (Eq. 8), $k \propto M^{2/3}$ at constant $\hat{x}$. The literature suggests that the stiffness of carnivoran footpads scales with an exponent closer to 1 (Chi and Louise Roth, 2010). The Hertz model cannot achieve this while also maintaining geometric (and thus dynamic) similarity: from Eq. (B.2), $k \propto M^1$ can be achieved by scaling $E^* \propto M^{2/3}$, which means Eq. (8) would no longer apply. Alternatively, $k \propto M^1$ can be achieved by relaxing the constraints on either R or $\hat{x}$, which would also deviate from geometric similarity.

Alexander et al. (1986) compared the mechanical properties of mammalian paw pads using a "dimensionless stiffness parameter". Accounting for a contact surface with multiple spheres, we can compute dimensionless stiffness $\hat{k}$ as:

$$\hat{k} = \frac{k \cdot R \cdot n_{\mathrm{spheres}}}{F_{\mathrm{e}}} \tag{B.3}$$

The linearised, undamped natural frequency (f_{n}, in Hz) of a Hertzian contact sphere supporting a mass M can be calculated as:

$$f_{\mathrm{n}} = \frac{1}{2\pi} \sqrt{\frac{k}{M}}, \tag{B.4}$$

which will be valid for small amplitude oscillations. In static equilibrium under gravity g, $F_{\mathrm{e,eq}} = M \cdot g$ in Eq. (3) of the main manuscript, implying that $M = F_{\mathrm{e,eq}}/g$. That means that we can calculate the equilibrium natural frequency as:

$$f_{\mathrm{n,eq}} = \frac{1}{2\pi} \sqrt{\frac{3\,k \cdot g}{4\,\eta \cdot R^2 \cdot E^* \cdot \hat{x}_{eq}^{3/2}}} = \frac{1}{2\pi} \sqrt{\frac{3}{2} \frac{1}{\hat{x}_{eq}} \frac{g}{R}} \tag{B.5}$$

The variable $\hat{x}_{eq}$ is the equilibrium normalised indentation, which is kept constant through the scaling approach applied in this manuscript.

Appendix C. SmoothSphereHalfSpaceForce in OpenSim

OpenSim includes "SmoothSphereHalfSpaceForce", which is a smoothed version of the standard HuntCrossleyForce, developed specifically for increased performance in gradient-based optimisations (Serrancoli et al., 2019; Dembia et al., 2020). The elastic (Hertz) portion of the contact model is smoothed in two ways: 1) by addition of the term cf that ensures a low force even when there is no contact (thus preventing null-derivatives), and 2) by approximating the binary conditions of no contact/contact with a tanh function based on the contact indentation (preventing infinite derivatives). The entire model is also smoothed at the velocity level with a second tanh function to prevent negative contact forces. The smoothing parameters are not dimensionless, and thus their effects are sensitive to the scale of the contact parameters, unless the smoothing parameters are also scaled. Fig. C.5 shows that inappropriate combinations of parameters can lead to high contact forces well-before the actual contact is initiated (signified by the red shaded area in panel A). This can be interpreted as the contacts repelling the ground without contact, or alternatively as modelling larger contact spheres than intended. This issue occurs when the cf term is relatively high, combined with too smooth a tanh-transition, which together allow the constant contact force to bleed through before contact is actually initiated.

An interactive way to check whether this issue is present in a model is to load it into OpenSim Creator (Kewley et al., 2026), and to observe whether the real-time contact force visualisations build up substantially before the contact spheres intersect the contact halfspace. A MATLAB script that parametrically generates Fig. C.5 is provided in the supplementary materials, which enables plotting the effects of different scaling choices. In the next sections, I will present some derivations and physical interpretations of the smoothing parameters. I will also provide some practical recommendations on how to scale them, based on published models where the smoothing parameters apparently caused no issues.

C.1. Constant force due to cf

Inclusion of the parameter cf results in a rewritten version of Eq. (1) (Serrancoli et al., 2019):

$$F_{cf} = \frac{4}{3} \eta \cdot R^{1/2} \cdot E^* \cdot \sqrt{(x^2 + cf)}^{3/2} \tag{C.1}$$

While the parameter cf is named "constant_contact_force" in OpenSim, from its position in Eq. (C.1) it is perhaps more accurately described as a "constant contact indentation squared", with units m^2. This is an important distinction, because the indentation due to cf can result in drastically different force magnitudes depending on the contact sphere radius R (Eq. C.1). OpenSim's default value of 10^{-5} m^2 corresponds to a constant contact indentation of $x = 0.0032$ m, and it is advisable to scale the magnitude of cf with R. For instance, the mouse model simulated in this manuscript has $R = 0.002$ m. The default cf

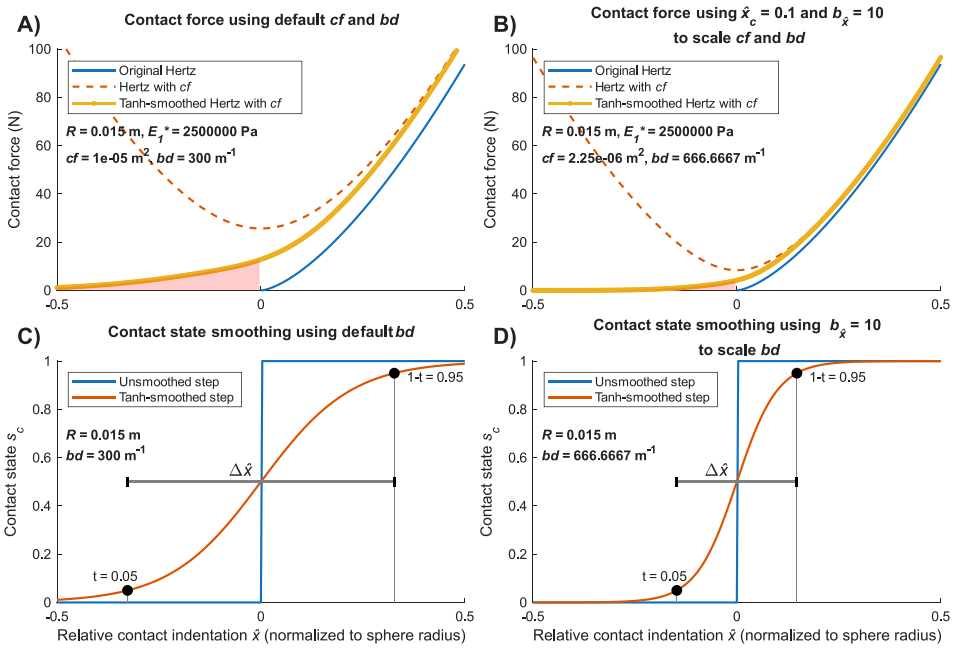

Fig. C.5. The smoothing parameters in OpenSim's "SmoothSphereHalfSpaceForce" are not dimensionless, and can cause issues when using relatively small contact spheres (here, $R = 0.015$ m). **A)** Using default values for the cf and bd parameters, the smooth contact model (yellow dotted line) produces substantial amounts of force before contact is initiated, signified by the red shaded area. The cf parameter, which effectively adds a constant contact indentation, resulting in the Hertz force with cf (dashed Orange line) being substantially higher than the regular Hertz force (blue line). Force builds up before contact initiation due to smoothing via bd which results in contact state buildup before physical contact (see panel C). **B)** After scaling, the smoothed force is much closer to the unsmoothed Hertz force, because lowering cf reduces the constant contact force, and raising bd reduces the transition width (see panel D). **C)** In the unsmoothed model, contact is a binary state, signified by a step function. This is smoothly approximated by a tanh function, which means contact is initiated before the sphere intersects the halfspace. The default value of bd encodes an absolute transition distance, which means that in small contact spheres, the smoothing has a much stronger effect. **D)** After scaling bd, the contact transition occurs over a much smaller fraction of the sphere radius. This prevents large forces bleeding through before contact is initiated. (For interpretation of the references to colour in this figure legend, the reader is referred to the web version of this article.)

would result in an indentation of more than 1.5 times the contact radius, causing the model to float in the air during steady-state. This would be obvious in such a small model, but is much more insidious in a medium sized model: the emu model used $R = 0.015$ m, and this issue can only be diagnosed by plotting the force indentation curve (Fig. C.5). One scaling approach would be to choose cf based on a desired level of constant relative indentation $\hat{x}_c$ (which is a fraction of R, and thus dimensionless):

$$cf = (R \cdot \hat{x}_c)^2 \tag{C.2}$$

Lower $\hat{x}_c$ then results in less constant indentation, and vice versa. Using the Falisse et al. (2022) human model's $R = 0.032$ m as a reference value, a possible starting point for $\hat{x}_c$ could be 0.0988, or simply 0.1, signifying a constant contact deformation of 10 % of the contact radius. Fig. C.5(B) demonstrates the effect of this scaling. If the recommendation of $\hat{x} < 0.16$ from the main manuscript is followed, $\hat{x}_c$ should be adjusted accordingly (e.g., 0.05).

C.2. Smoothing with tanh functions

The Hertz equation (Eq. 1) is only defined when the objects are actually in contact. Simulators can enact this by only computing the force if x is positive (negative x thus represents no contact). Such an "if statement" can be thought of as a binary step—when a contact sphere goes from zero indentation to a finite level of indentation, there is a binary step in the contact state from 0 to 1 (Fig. C.5C). The binary step (between 0 and 1, representing "no" and "some" contact, respectively) can be smoothly approximated by introducing a smoothed contact state $s_c(x)$, which is a function of x. Then, the smoothed Hertz force F_s can be computed as follows:

$$F_s = F_{cf} \cdot s_c(x) \tag{C.3}$$

In the unsmoothed model, contact is binary, and thus no forces are produced when there are no intersections. In the smoothed model, the contact state $s_c(x)$ is continuous between 0 and 1, as a function of indentation x. In SmoothSphereHalfSpaceForce (Dembia et al., 2020; Serrancoli et al., 2019), the smoothing is achieved with a tanh function:

$$s_c(x) = 0.5 + 0.5 \cdot \tanh(bd \cdot x) \tag{C.4}$$

See also Fig. C.5C, where s_c is plotted as a function of $\hat{x}$. The parameter bd, called "hertz_smoothing" in OpenSim, determines how smooth the transition is between 0 and 1. By the nature of this function, $s_c(x)$ tends asymptotically to 0 for negative x, asymptotically to 1 for positive x, and is exactly 0.5 when $x = 0$. In other words, the tanh-approximation results in the contact state building up before the sphere actually intersects the halfspace. Because F_{cf} is non-zero before the spheres intersect (due to the constant force caused by cf), the smoothed contact force F_s will also be non-zero before the spheres intersect (Eq. C.3). While this behaviour is intentional (to improve gradient based optimizations (Serrancoli et al., 2019)), it is not scale invariant: Eq. (C.4) implies bd has units m^{-1}, the reciprocal of the length scale, because $s_c(x)$ itself is dimensionless. Thus, the smoothing enacted by bd is not dimensionless, the transition from "no contact" to "contact" will always occur over the same absolute distance, whereas the investigator is likely to tailor R to the scale of the model.

The OpenSim default value of parameter bd (300 m^{-1}) will have relatively little smoothing effect for large R (e.g., $R >$ 0.06 m), but small values of R (e.g., $R <$ 0.02 m) are more problematic, especially if cf was not scaled (compare the shaded areas in Fig. C.5A and B). Based on its placement in Eq. (C.4), it is clear that bd should be scaled according to $bd \propto R^{-1}$. This can be used to scale bd between different models. To

specify an arbitrarily steep transition:

$$bd = \frac{b_{\hat{x}}}{R}, \tag{C.5}$$

where $b_{\hat{x}}$ is a dimensionless smoothing parameter that controls the relative indentation $\hat{x}$ over which any given fraction of the $s_c(x)$ step occurs (derived below). The Falisse et al. (2022) model does not have the smoothing issue, and used $bd = 300\ \mathrm{m}^{-1}$, with $R = 0.032$ m. This implies that a suitable starting value for $b_{\hat{x}}$ could be $300 \cdot 0.032 = 9.6$, or simply 10. Setting $b_{\hat{x}} = 10$ would imply that the smoothed step function increases from 5 % to 95 % when $\hat{x}$ varies from -0.15 to 0.15 radius fractions (see Eq. (C.8) below, and Fig. C.5(C) and D).

Eq. (C.4) can be rewritten to estimate a suitable $b_{\hat{x}}$ with more fine-grained control, allowing us to specify the fraction of the radius that should correspond to a desired increase in the contact state. To do this, we introduce a variable t that defines a threshold on our (smoothed) step function, with a corresponding relative indentation $\hat{x}_t$ at which the threshold occurs. For instance, if we desire our step function to reach 95% for an arbitrary relative indentation $\hat{x}_t$, we choose $t = 0.05$, and set our threshold as follows: $s_c = 1 - t$ (Fig. C.5C and D). We can insert this into Eq. (C.4), once again using Eq. (2) to normalise x, and solve for $\hat{x}_t$. This gives:

$$\hat{x}_t = \frac{\mathrm{atanh}(1 - 2t)}{bd \cdot R} \tag{C.6}$$

Because Eq. (C.4) is symmetric about the point (0, 0.5), we can use the above to define a width in $\hat{x}$ over which the transition between $s_c = t$ and $s_c = 1 - t$ occurs:

$$\Delta\hat{x} = \frac{2\mathrm{atanh}(1 - 2t)}{bd \cdot R} \tag{C.7}$$

For example, if $t = 0.05$, $\Delta\hat{x}$ defines the negative to positive indentation which encompasses 90 % of the total step function (because it is symmetric about 0.5, Fig. C.5C and D). Note that $\Delta\hat{x} = 2\hat{x}_t$, because the smooth contact state s_c builds up before the sphere intersects the halfspace. Rewriting the above equation to solve for bd, we acquire:

$$bd = \frac{2\mathrm{atanh}(1 - 2t)}{\Delta\hat{x} \cdot R}. \tag{C.8}$$

This shows that $b_{\hat{x}}$ from Eq. (C.5) can be parameterised as $\frac{2\mathrm{atanh}(1-2\ t)}{\Delta\hat{x}}$. $1 - 2t$ can be interpreted as the percentage of the step that is traversed over $\Delta\hat{x}$, the relative indentation over which it occurs. In the limit for $1 - 2t$ to 1 and $\Delta\hat{x}$ to 0, the step function is no longer an approximation, but also no longer smooth. Thus, if specifying bd (or $b_{\hat{x}}$) this way, care should be taken that the selected t and $\hat{x}_t$ are neither too small nor too large. The supplementary data repository contains a MATLAB script that allows plotting the effects of different combinations of $\hat{x}_c$ and $b_{\hat{x}}$.

In SmoothSphereHalfSpaceForce, the total normal force is subjected to a second layer of smoothing, with $\dot{x}$ as the input variable (Serrancoli et al., 2019; Dembia et al., 2020). This is to ensure that the dissipative (Hunt–Crossley) force can never cause negative contact forces (sticking). This is achieved by centering the tanh at the speed where $F_\mathrm{d} = -F_\mathrm{e}$, which occurs at $\dot{x} = -\frac{2}{3\alpha}$ (see Eq. (12)), and introducing a second smoothing parameter bv, called "hunt_crossley_smoothing" (default value = 50 s / m). In equation form:

$$F_{\text{total, smooth}} = (F_s + 3/2F_s \cdot \alpha \cdot \dot{x})(0.5 + 0.5 \cdot \tanh(bv(\dot{x} + \frac{2}{3\alpha}))) \tag{C.9}$$

The term between the first brackets is the smoothed equivalent of $F_\mathrm{e} + F_\mathrm{d}$, and the second term is the velocity smoothing term. The full derivation is left as an exercise to the reader, because by analogy with Eqs. (C.5) and (C.8), we can see that bv has units s / m, scales according to $bv \propto R^{-1/2}$, and can be customised as follows:

$$bv = \frac{b_{\dot{\hat{x}}}}{R^{1/2}} = \frac{2\mathrm{atanh}(1 - 2t)}{\Delta\dot{\hat{x}}R^{1/2}}. \tag{C.10}$$

Again referencing the Falisse et al. (2022) model, a starting point for $b_{\dot{\hat{x}}}$ could be $50 \cdot 0.032^{1/2} = 8.94$, or simply 9.

Scaling bv may have very little effect in practice, unless the movement that is being simulated has very high negative $\dot{x}$ (e.g., a high takeoff velocity).

Appendix D. Supplementary data

Supplementary data to this article can be found online at doi:10.1016/j.jbiomech.2026.113420.

Data availability

The OpenSim models and simulation code (that also produce Figs. 1, 4, C.5) have been uploaded to a dedicated online repository at doi:10.5281/zenodo.20730121.

References

Aerts, P., Ker, R., De Clercq, D., Ilsley, D., Alexander, R.McN., 1995. The mechanical properties of the human heel pad: a paradox resolved. J. Biomech. 28, 1299–1308. https://doi.org/10.1016/0021-9290(95)00009-7

Afschrift, M., Kistemaker, D., Bobbert, M., De Groote, F., 2025. Benchmarking the predictive capability of human gait simulations. PLOS Comput. Biol. 21, e1012713. https://doi.org/10.1371/journal.pcbi.1012713

Alexander, R.McN., 2006. Principles of Animal Locomotion. Princeton University Press, Princeton NJ.

Alexander, R.McN., Jayes, A.S., 1983. A dynamic similarity hypothesis for the gaits of quadrupedal mammals. J. Zool. 201, 135–152. https://doi.org/10.1111/j.1469-7998.1983.tb04266.x

Alexander, R.McN., Bennett, M.B., Ker, R.F., 1986. Mechanical properties and function of the PAW pads of some mammals. J. Zool. 209, 405–419. https://doi.org/10.1111/j.1469-7998.1986.tb03601.x

Baines, P.M., Schwab, A.L., van Soest, A.J., 2018. Experimental estimation of energy absorption during heel strike in human barefoot walking. PLoS One 13, e0197428. https://doi.org/10.1371/journal.pone.0197428

Bates, K.T., Falkingham, P.L., 2012. Estimating maximum bite performance in *Tyrannosaurus rex* using multi-body dynamics. Biol. Lett. 8, 660–664. https://doi.org/10.1098/rsbl.2012.0056

Bates, K.T., McCormack, S., Donald, E., Coatham, S., Brassey, C.A., Charles, J., O'Mahoney, T., van Bijlert, P.A., Sellers, W.I., 2025. Running performance in *Australopithecus afarensis*. Curr. Biol. 35, 224–230.e4. https://doi.org/10.1016/j.cub.2024.11.025

Bianco, N.A., Collins, S.H., Liu, K., Delp, S.L., 2023. Simulating the effect of ankle plantarflexion and inversion-eversion exoskeleton torques on center of mass kinematics during walking. PLOS Comput. Biol. 19, e1010712. https://doi.org/10.1371/journal.pcbi.1010712

Charles, J.P., Cappellari, O., Spence, A.J., Wells, D.J., Hutchinson, J.R., 2016. Muscle moment arms and sensitivity analysis of a mouse hindlimb musculoskeletal model. J. Anat. 229, 514–535. https://doi.org/10.1111/joa.12461

Charles, J.P., Kissane, R.W.P., Askew, G.N., 2024. The impacts of muscle-specific force-velocity properties on predictions of mouse muscle function during locomotion. Front. Bioeng. Biotechnol. 12, 1436004. https://doi.org/10.3389/fbioe.2024.1436004

Chi, K.J., Louise Roth, V., 2010. Scaling and mechanics of carnivoran footpads reveal the principles of footpad design. J. R. Soc. Interface 7, 1145–1155. https://doi.org/10.1098/rsif.2009.0556

Clemente, C.J., De Groote, F., Dick, T.J.M., 2024. Predictive musculoskeletal simulations reveal the mechanistic link between speed, posture and energetics among extant mammals. Nat. Commun. 15, 8594. https://doi.org/10.1038/s41467-024-52924-z

Daley, M.A., Birn-Jeffery, A., 2018. Scaling of avian bipedal locomotion reveals independent effects of body mass and leg posture on gait. J. Exp. Biol. 221, jeb152538. https://doi.org/10.1242/jeb.152538

De Groote, F., Kinney, A.L., Rao, A.V., Fregly, B.J., 2016. Evaluation of direct collocation optimal control problem formulations for solving the muscle redundancy problem. Ann. Biomed. Eng. 44, 2922–2936. https://doi.org/10.1007/s10439-016-1591-9

Dembia, C.L., Bianco, N.A., Falisse, A., Hicks, J.L., Delp, S.L., 2020. OpenSim MOCO: musculoskeletal optimal control. PLOS Comput. Biol. 16, e1008493. https://doi.org/10.1371/journal.pcbi.1008493

D'Hondt, L., De Groote, F., Afschrift, M., 2024a. A dynamic foot model for predictive simulations of human gait reveals causal relations between foot structure and whole-body mechanics. PLOS Comput. Biol. 20, e1012219. https://doi.org/10.1371/journal.pcbi.1012219

D'Hondt, L., Falisse, A., Gupta, D., Van Den Bosch, B., Buurke, T.J.W., Febrer-Nafría, M., Vandekerckhove, I., Afschrift, M., De Groote, F., 2024b. PredSim: a framework for rapid predictive simulations of locomotion. In: 2024 10th IEEE RAS/EMBS International Conference for Biomedical Robotics and Biomechatronics (BioRob). IEEE, Heidelberg, Germany, pp. 1208–1213, https://doi.org/10.1109/BioRob60516.2024.10719735

Ding, S., Hu, Y., Jian, B., Zhang, Y., Xia, R., Hu, G., 2024. A review and comparative analysis of normal contact force models for viscoelastic particles. Int. J. Impact Eng. 189, 104968. https://doi.org/10.1016/j.ijimpeng.2024.104968

Falisse, A., Afschrift, M., De Groote, F., 2022. Modeling toes contributes to realistic stance knee mechanics in three-dimensional predictive simulations of walking. PLoS One 17, e0256311. https://doi.org/10.1371/journal.pone.0256311

Gong, H., Zhang, C., Sui, Y., 2025. Contact-rich and deformable foot modeling for locomotion control of the human musculoskeletal system. arxiv:2508.11885

Gonthier, Y., McPhee, J., Lange, C., Piedbœuf, J.C., 2004. A regularized contact model with asymmetric damping and dwell-time dependent friction. Multibody Syst. Dyn. 11, 209–233. https://doi.org/10.1023/B:MUBO.0000029392.21648.bc

Grant, B., Charles, J., Geraghty, B., Gardiner, J., D'Août, K., Falkingham, P.L., Bates, K.T., 2022. Why does the metabolic cost of walking increase on compliant substrates? J. R. Soc. Interface 19, 20220483. https://doi.org/10.1098/rsif.2022.0483

Hao, K.A., Nichols, J.A., 2021. Simulating finger-tip force using two common contact models: hunt-crossley and elastic foundation. J. Biomech. 119, 110334. https://doi.org/10.1016/j.jbiomech.2021.110334

Hertz, H., 1893. Electric Waves: Being Researches on the Propagation of Electric Action with Finite Velocity Through Space. Cornell University Library, New York.

Hertz, H., 1896. On the contact of elastic solids. In: Lenard, P. (Ed.), Miscellaneous Papers. Macmillan and Co, London, pp. 146–162.

Hunt, K.H., Crossley, F.R.E., 1975. Coefficient of restitution interpreted as damping in vibroimpact. J. Appl. Mech. 42, 440–445. https://doi.org/10.1115/1.3423596

Johnson, K.L. ed), 1985. Contact Mechanics, 1 ed. Cambridge University Press, https://doi.org/10.1017/CBO9781139171731

Kerdok, A.E., Biewener, A.A., McMahon, T.A., Weyand, P.G., Herr, H.M., 2002. Energetics and mechanics of human running on surfaces of different stiffnesses. J. Appl. Physiol. 92, 469–478. https://doi.org/10.1152/japplphysiol.01164.2000

Kewley, A., van Beesel, J., Seth, A., 2026. OpenSim creator: an interactive user interface for building OpenSim musculoskeletal models. J. Open Source Softw. 11, 8284. https://doi.org/10.21105/joss.08284

Lin, D.C., Shreiber, D.I., Dimitriadis, E.K., Horkay, F., 2009. Spherical indentation of soft matter beyond the hertzian regime: numerical and experimental validation of hyperelastic models. Biomech. Model. Mechanobiol. 8, 345–358. https://doi.org/10.1007/s10237-008-0139-9

McConnochie, G.E., Fox, A., Bellenger, C., Thewlis, D., 2026. Metabolic and biomechanical responses to running-related fatigue assessed with optimal control simulations tracking wearable sensor signals. R. Soc. Open Sci. 13, 250668. https://doi.org/10.1098/rsos.250668

McMahon, T.A., Greene, P.R., 1979. The influence of track compliance on running. J. Biomech. 12, 893–904. https://doi.org/10.1016/0021-9290(79)90057-5

Michilsens, F., Aerts, P., Van Damme, R., D'Août, K., 2009. Scaling of plantar pressures in mammals. J. Zool. 279, 236–242. https://doi.org/10.1111/j.1469-7998.2009.00611.x

Millard, M., Mombaur, K., 2019. A quick turn of foot: rigid foot-ground contact models for human motion prediction. Front. Neurorobotics 13, 62. https://doi.org/10.3389/fnbot.2019.00062

Miller, R.H., Bell, E.M., Russell Esposito, E., 2024. Transfemoral limb loss modestly increases the metabolic cost of optimal control simulations of walking. PeerJ 12, e16756. https://doi.org/10.7717/peerj.16756

Prescott, T.L., Griffin, B.W., Demuth, O.E., Gatesy, S.M., Lallensack, J.N., Falkingham, P.L., 2025. Speed from fossil trackways: calculations not validated by extant birds on compliant substrates. Biol. Lett. 21, 20250191. https://doi.org/10.1098/rsbl.2025.0191

Rodrigues Da Silva, M., Marques, F., Tavares Da Silva, M., Flores, P., 2022. A compendium of contact force models inspired by hunt and crossley's cornerstone work. Mech. Mach. Theory 167, 104501. https://doi.org/10.1016/j.mechmachtheory.2021.104501

Sellers, W., Margetts, L., Bates, K., Chamberlain, A., 2013. Exploring diagonal gait using a forward dynamic three-dimensional chimpanzee simulation. Folia Primatol. 84, 180–200. https://doi.org/10.1159/000351562

Serrancoli, G., Falisse, A., Dembia, C., Vantilt, J., Tanghe, K., Lefeber, D., Jonkers, I., De Schutter, J., De Groote, F., 2019. Subject-exoskeleton contact model calibration leads to accurate interaction force predictions. IEEE Trans. Neural Syst. Rehabil. Eng. 27, 1597–1605. https://doi.org/10.1109/TNSRE.2019.2924536

Seth, A., Hicks, J.L., Uchida, T.K., Habib, A., Dembia, C.L., Dunne, J.J., Ong, C.F., DeMers, M.S., Rajagopal, A., Millard, M., Hamner, S.R., Arnold, E.M., Yong, J.R., Lakshmikanth, S.K., Sherman, M.A., Ku, J.P., Delp, S.L., 2018. OpenSim: simulating musculoskeletal dynamics and neuromuscular control to study human and animal movement. PLOS Comput. Biol. 14, e1006223. https://doi.org/10.1371/journal.pcbi.1006223

Sherman, M.A., Seth, A., Delp, S.L., 2011. Simbody: multibody dynamics for biomedical research. Procedia IUTAM 2, 241–261. https://doi.org/10.1016/j.piutam.2011.04.023

Skrinjar, L., Slavič, J., Boltežar, M., 2018. A review of continuous contact-force models in multibody dynamics. Int. J. Mech. Sci. 145, 171–187. https://doi.org/10.1016/j.ijmecsci.2018.07.010

van Bijlert, P.A., 2024. MuSkeMo: open-source software to construct, analyze, and visualize human and animal musculoskeletal models and movements in Blender. bioRxiv (preprint) https://doi.org/10.1101/2024.12.10.627828

van Bijlert, P.A., Geijtenbeek, T., Smit, I.H., Schulp, A.S., Bates, K.T., 2024a. Muscle-driven predictive physics simulations of quadrupedal locomotion in the horse. Integr. Comp. Biol. 64, 694–714. https://doi.org/10.1093/icb/icae095

van Bijlert, P.A., van Soest, A.J., Schulp, A.S., Bates, K.T., 2024b. Muscle-controlled physics simulations of bird locomotion resolve the grounded running paradox. Sci. Adv. 10, eado0936. https://doi.org/10.1126/sciadv.ado0936

van den Bogert, A., Schamhardt, H., Crowe, A., 1989. Simulation of quadrupedal locomotion using a rigid body model. J. Biomech. 22, 33–41. https://doi.org/10.1016/0021-9290(89)90182-6

van den Bogert, A.J., Blana, D., Heinrich, D., 2011. Implicit methods for efficient musculoskeletal simulation and optimal control. Procedia IUTAM 2, 297–316. https://doi.org/10.1016/j.piutam.2011.04.027

van Soest, A.J., Schwab, A.L., Bobbert, M.F., van Ingen Schenau, G.J., 1993. The influence of the biarticularity of the gastrocnemius muscle on vertical-jumping achievement. J. Biomech. 26, 1–8. https://doi.org/10.1016/0021-9290(93)90608-H

Watson, P.J., Gröning, F., Curtis, N., Fitton, L.C., Herrel, A., McCormack, S.W., Fagan, M.J., 2014. Masticatory biomechanics in the rabbit: a multi-body dynamics analysis. J. R. Soc. Interface 11, 20140564. https://doi.org/10.1098/rsif.2014.0564